Regular Article

Highlighted Paper selected by Editor-in-Chief

Synthesis and Characterization of Hydroxyethylamino- and Pyridyl-Substituted 2-Vinyl Chromone Derivatives for Detection of Cerebral Abnormal Prion Protein Deposits

Mari Nakaie,[a] Fumihiro Katayama,[a] Takehiro Nakagaki,[b] Masao Kawasaki,[a] Sakura Yoshida,[a] Akira Toriba,[a] Kazuma Ogawa,[c,d] Noriyuki Nishida,[b] Morio Nakayama,*,[a] and Takeshi Fuchigami*,[a,c]

[a] *Department of Hygienic Chemistry, Graduate School of Biomedical Sciences, Nagasaki University; 1–14 Bunkyo-machi, Nagasaki 852–8521, Japan:* [b] *Department of Molecular Microbiology and Immunology, Graduate School of Biomedical Sciences, Nagasaki University; 1–12–4 Sakamoto, Nagasaki 852–8523, Japan:* [c] *Laboratory of Clinical Analytical Sciences, Graduate School of Medical Sciences, Kanazawa University; Kakuma-machi, Kanazawa, Ishikawa 920–1192, Japan: and* [d] *Institute for Frontier Science Initiative, Kanazawa University; Kanazawa, Ishikawa 920–1192, Japan.*
Received October 19, 2021; accepted December 14, 2021

Prion diseases are fatal neurodegenerative diseases characterized by the deposition of abnormal prion protein aggregates (PrP^{Sc}) in the brain. In this study, we developed hydroxyethylamino-substituted styryl-chromone (SC) and 2-(2-(pyridin-3-yl)vinyl)-4*H*-chromen-4-one (VPC) derivatives for single-photon emission computed tomography (SPECT) imaging of PrP^{Sc} deposits in the brain. The binding affinity of these compounds was evaluated using recombinant mouse prion protein (rMoPrP) aggregates, which resulted in the inhibition constant (K_i) value of 61.5 and 88.0 nM for hydroxyethyl derivative, (*E*)-2-(4-((2-hydroxyethyl)amino)styryl)-6-iodo-4*H*-chromen-4-one (SC-NHEtOH) and (*E*)-2-(4-((2-hydroxyethyl)(methyl)amino)styryl)-6-iodo-4*H*-chromen-4-one (SC-NMeEtOH), respectively. However, none of the VPC derivatives showed binding affinity for the rMoPrP aggregates. Fluorescent imaging demonstrated that the accumulation pattern of SC-NHEtOH matched with the presence of PrP^{Sc} in the brain slices from mouse-adapted bovine spongiform encephalopathy-infected mice. A biodistribution study of normal mice indicated low initial brain uptake of [^{125}I]SC-NHEtOH (0.88% injected dose/g (% ID/g) at 2 min) despite favorable washout from the brain (0.26% ID/g, at 180 min) was displayed. [^{125}I]SC-NHEtOH exhibited binding affinities to both artificial prion aggregates as well as prion deposits in the brain. However, significant improvement in the binding affinity for PrP^{Sc} and blood–brain barrier permeability is necessary for the development of successful *in vivo* imaging probes for the detection of cerebral PrP^{Sc} in the brain.

Key words prion disease; scrapie prion protein (PrP^{Sc}); 2-vinyl chromone; single-photon emission computed tomography (SPECT)

Introduction

Infectious spongiform encephalopathy, commonly known as prion disease, is a fatal transmissible neurodegenerative disease in both humans and animals.[1] Neurodegenerative disorders such as Creutzfeldt–Jakob disease (CJD), fatal familial insomnia (FFI), Kuru, and Gerstmann–Straussler–Scheinker syndrome (GSS), are known human prion diseases. Bovine spongiform encephalopathy (BSE) in cattle and chronic wasting disease (CWD) in deer are known animal prion diseases.[2] Neuropathological features of prion disease include abnormal accumulation of prion proteins in the brain, vacuolization of the corpus cavernosum, and severe loss of neurons.[3] These diseases show the unique characteristic of being caused by a variety of factors, including infectious molecules and endogenous factors. It has been found that misfolding and aggregation of the normal cellular prion protein PrP (PrP^C) produces pathogenic scrapie PrP (PrP^{Sc}), which accumulates in the brain resulting in the prion disease progression.[4] PrP^C is a glycoproteins present on the cell surface that is rich in α-helix, whereas PrP^{Sc} has abundant β-sheet content and propagation properties.[5] It has been reported that PrP^C protects neurons from Ca^{2+} overload through regulation of ionotropic gluta-mate receptor function. However, PrP^{Sc} showed neurotoxic effects *via* *N*-methyl-D-aspartate (NMDA)- and α-amino-3-hydroxy-5-methyl-4-isoxazolepropionic acid receptor-mediated increases in calcium signaling, including depolymerizing actin filaments in dendritic spines, albeit the mechanism of prion disease still remains elusive.[6] The unequivocal diagnosis of prion disease now relies on the detection of PrP^{Sc} in post-mortem brain tissue.[7] Real-time quaking-induced conversion (RT-QUIC) is an *in vitro* diagnostic method based on the PrP^{Sc} amplification assay that enables the detection of PrP^{Sc} in the clinical samples containing cerebrospinal fluid or olfactory mucosa of patients suspected of having prion diseases. Recently, RT-QUIC has been used as a diagnostic criterion for the clinical diagnosis of sporadic CJD.[8–10] Another neurodegenerative feature of the disease is amyloid plaques containing PrP^{Sc} in the brain tissue.[11,12] Positron emission tomography (PET) and single-photon emission computed tomography (SPECT) and are non-invasive nuclear medicine diagnosis methods that can detect various pathological molecules of central nervous system (CNS) disorders including prion deposits in the brain.[13,14] Visualization of PrP^{Sc} deposits in the living human brain could identify sites of PrP^{Sc} and monitor
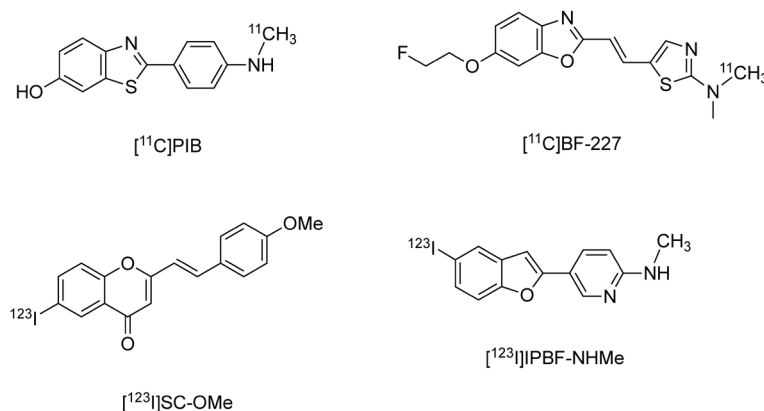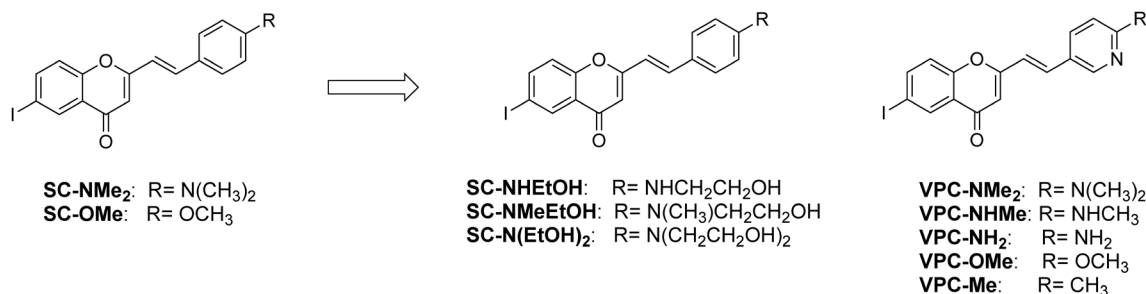
Fig. 1. Chemical Structures of Previously Reported Prion Imaging Probes

Fig. 2. Design of Novel 2-Vinyl Chromones as PrP^{Sc} Imaging Probes in This Study

the progression of prion diseases and their characteristics. As PrP^{Sc} is rich in beta-sheets similar to beta-amyloid (Aβ) plaques that are characteristic of Alzheimer's disease (AD),[15] several studies have been performed to visualize PrP^{Sc} in prion disease patients using various radioligands targeting Aβ. However, inconsistent results, including some samples and negative reports, have impeded the confirmation of their validation in clinical practice.[16] In fact, the Aβ imaging agents [^{11}C]BF-227 and [^{11}C]PIB failed to visualize patients with CJD and GSS, respectively.[17,18] Recently, we developed several series of radioligands, including flavonoids,[19] quinacrines,[20] and benzofurans[21,22] as new prion imaging probes (Fig. 1). Among them, [^{123}I]SC-OMe, a flavonoid-related styrylchromone (SC) derivative, demonstrated consistent accumulation with the distribution of PrP^{Sc} in the brain tissue of mouse-adapted BSE (mBSE)-infected mice by SPECT/CT imaging.[19] More recently, we reported that SPECT imaging using pyridyl benzofuran derivative [^{123}I]IPBF-NHMe visualized prion deposition in mBSE-infected mice.[21] However, relatively inadequate blood–brain barrier (BBB) permeability of [^{123}I]SC-OMe and the lack of amyloid specificity of [^{123}I]IPBF-NHMe may be obstacles for the clinical diagnosis of prion diseases. Therefore, specific and sensitive *in vivo* imaging of PrP^{Sc} requires further efforts to develop new imaging agents with improved brain distribution, binding affinity, or both.
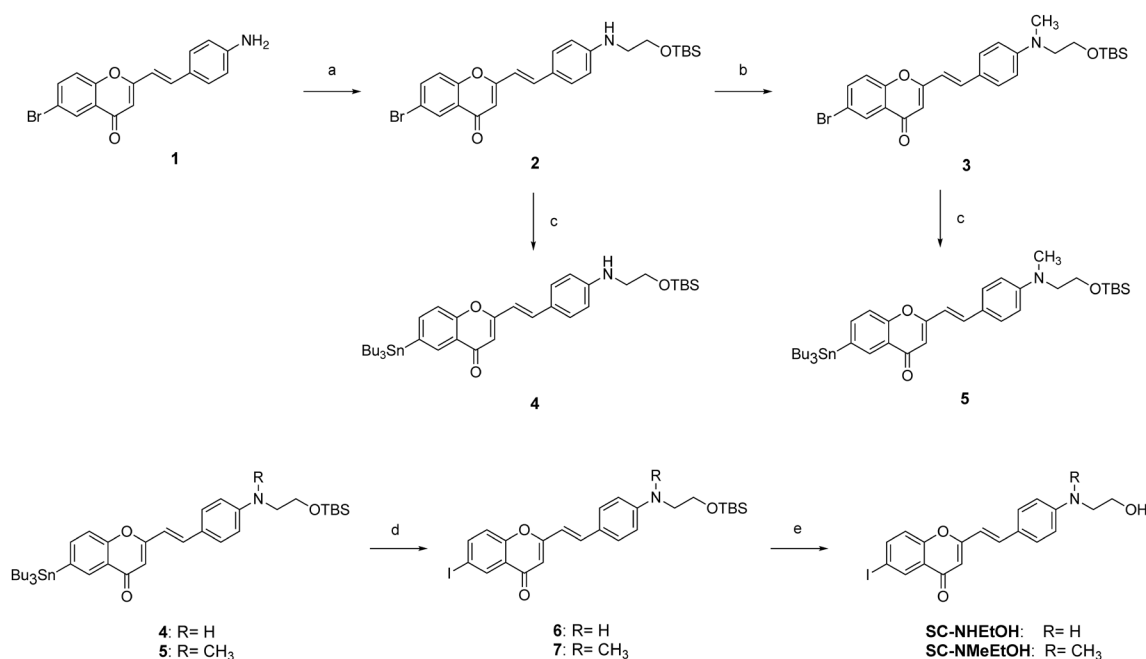
We here designed five 2-vinyl chromone derivatives as novel PrP^{Sc} imaging probes as shown in Fig. 2. A central nervous system multiparameter PET optimization (CNS PET MPO) algorithm has been used as a useful method for the design and selection of useful CNS PET agents.[23,24] Therefore, we have utilized this algorithm to design and discuss the *in vivo* pharmacokinetics of our recently developed imag-

ing probes.[21,22] This algorithm includes $C\log P$ (calculated $\log P$), $C\log D$ (calculated distribution coefficient at pH = 7.4), molecular weight (MW), topological polar surface area (TPSA), number of hydrogen bond donors (HBD), and pK_a (ionization constant of the most basic center). The favorable ranges are set as $C\log P \leq 2.8$, $C\log D \leq 1.7$, MW ≤ 305.3, $44.8 < \text{TPSA} \leq 63.3$, HBD ≤ 1, and p$K_a \leq 7.2$. The score range for each parameter is 0.0 to 1.0. It is reported that most successful CNS PET tracers have CNS PET MPO scores of over 3.[23] Table 1 shows CNS PET MPO scores of SC-related compounds which indicated that previously developed SC-NMe$_2$ and SC-OMe have unfavorable lipophilicity and TPSA values. IPBF-NHMe has more favorable lipophilicity and CNS PET MPO scores, indicating high BBB permeability.[21] However, it is presumed that many benzofuran derivatives have non-selective amyloid binding properties according to our previous reports.[21,22] On the other hand, several compounds showing higher selectivity for PrP^{Sc} have been found among chromone derivatives.[19] Thus, we designed novel SC derivatives (SC-NHEtOH, SC-NMeEtOH, and SC-N(EtOH)$_2$) and 2-(2-(pyridin-3-yl)vinyl)-4*H*-chromen-4-one (VPC) derivatives (VPC-NMe$_2$, VPC-NHMe, VPC-NH$_2$, VPC-OMe, and VPC-Me) with more favorable lipophilicity, TPSA values, and CNS PET MPO scores (Fig. 2 and Table 1). Indeed, the scores of the newly designed SC derivatives shown in Fig. 2 are close to 3, except for SC-N(EtOH)$_2$, suggesting their utility as *in vivo* imaging agents for PrP^{Sc}. In this study, we decided to develop SC-NHEtOH and SC-NMeEtOH as well as VPC-NMe$_2$ and VPC-OMe as candidate prion-imaging probes because of their ease of synthesis and high CNC PET MPO scores. VPC-NHMe having a substituent similar to IPBF-NHMe was calculated to have a high CNS PET MPO score. However, because

Table 1. Individual CNS PET MPO Parameters of Designed 2-Vinyl Chromones

Compound	$C\log P^{a)}$	$C\log D^{b)}$	TPSA$^{a)}$	MW	HBD	$pK_a{}^{b)}$	CNS PET MPO$^{c)}$
SC-NMe$_2$	4.55	5.75	29.54	417.25	0	3.35	2.00
SC-OMe	4.14	6.00	35.53	404.20	0	9.7	1.30
IPBF-NHMe$^{d)}$	3.61	4.93	33.62	350.2	1	4.61	2.40
SC-NHEtOH	3.25	5.04	58.56	433.25	2	3.18	2.60
SC-NMeEtOH	4.04	5.45	49.77	447.27	1	2.98	3.00
SC-N(EtOH)$_2$	3.52	4.58	70.00	477.30	2	2.39	2.10
VPC-NMe$_2$	3.93	5.48	41.90	418.23	0	5.60	2.80
VPC-NHMe	3.14	5.27	50.69	404.21	1	5.50	3.70
VPC-NH$_2$	2.84	4.76	64.88	390.18	2	5.48	2.90
VPC-OMe	3.52	4.90	47.89	405.19	0	1.97	3.20
VPC-Me	3.63	4.78	38.66	389.19	0	4.86	2.80

a) The physicochemical properties of each compound was calculated using a ChemDraw 20.1. *b*) The physicochemical properties of each compound was calculated using a SPARC on line calculator. *c*) The CNS PET MPO of each compound was calculated according to the literature.[23] $C\log P$, calculated partition coefficient; $C\log D$, calculated distribution coefficient at pH = 7.4; MW, molecular weight; TPSA, topological polar surface area; HBD, number of hydrogen bond donors, pK_a, ionization constant of the most basic center. *d*) Data from ref. 21).

Reagents and conditions: (a) (2-Bromoethoxy)-*tert*-butyldimethylsilane, K$_2$CO$_3$, DMF, 70 °C, 48 h; (b) (CH$_2$O)$_n$, NaCNBH$_3$, AcOH, room temperature (r.t.), 3 h; (c) (SnBu$_3$)$_2$, Pd(PPh$_3$)$_4$, dioxane, TEA, 90 °C, 7–12 h; (d) I$_2$, CHCl$_3$, (r.t.), 1–2 h; (e) TBAF, THF, 1–2 h.

Chart 1. Synthesis of Hydroxyethyl-Substituted 2-Vinyl Chromones

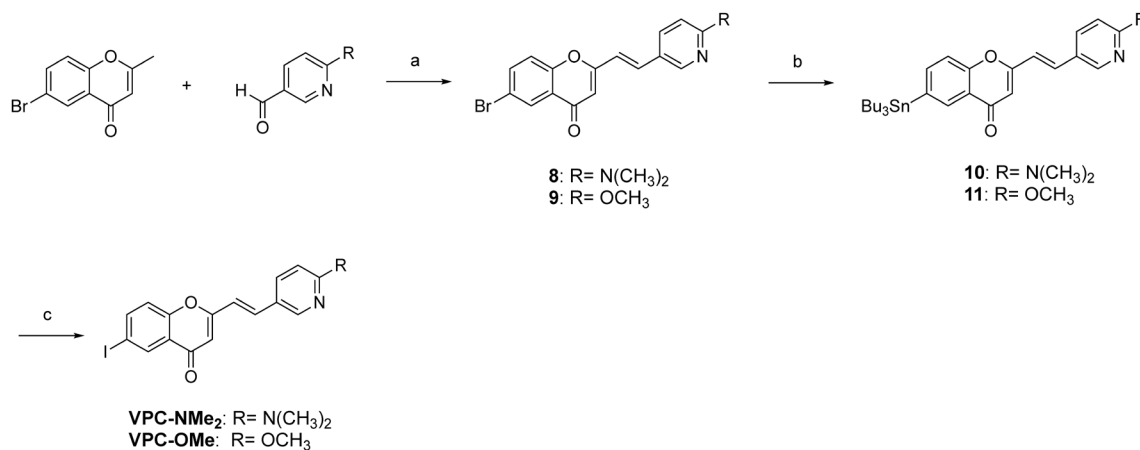of its complex synthesis, it was not included in this study.

Results and Discussion

Hydroxyethylamino-substituted SC derivatives (SC-NHEtOH and SC-NMeEtOH) were prepared as shown in Chart 1. Compound **1** was prepared according to the literature.[25] Alkylation of **1** with (2-bromoethoxy)-*tert*-butyldimethylsilane formed **2** in 41% yield. Methylation of the amine group of **2** was conducted using paraformaldehyde, acetic acid, and sodium cyanoborohydride (NaBH$_4$) which produced **3** in 51% yield. Treatment of **2** and **3** with tetrakis-(triphenylphosphine)-palladium(0) [(PPh$_3$)$_4$Pd] and bis(tributyltin) [(SnBu$_3$)$_2$] formed the tributyltin derivatives **4** and **5** in 18 and 23% yields, respectively. Iodine derivatives **6** and **7** were obtained by iodo-destannylation of **4** and **5** at yields of 45 and 73%, re-

spectively. Each *tert*-butyldimethylsilyl (TBS) group of **6** and **7** was deprotected with tetrabutylammonium fluoride (TBAF) which provided the target SC-NHEtOH and SC-NMeEtOH (22 and 58% yields, respectively).

The synthesis of the VPC derivatives is presented in Chart 2. Aldol reaction of 6-(*N,N*-dimethylamino)nicotinaldehyde or 6-methoxynicotinaldehyde with 6-bromo-2-methylchromone formed **8** and **9** at yields of 89 and 80%, respectively. These 2-(pyridin-3-yl-vinyl)chromones were converted to tributyltin derivatives **10** and **11** using a bromo-to-tributyltin exchange reaction catalyzed by Pd(0) in yields of 6 and 29%, respectively. The tributyltin derivatives **10** and **11** were reacted with iodine in CHCl$_3$ to form the target iodo derivatives VPC-NMe$_2$ and VPC-OMe (97 and 91% yield, respectively).

In our previous studies, we used rMoPrP aggregates as

Reagents and conditions: (a) KOH, EtOH, 70 °C, 4 h; (b) (SnBu$_3$)$_2$, Pd(PPh$_3$)$_4$, dioxane, TEA, 90 °C, 8–11 h; (c) I$_2$, CHCl$_3$, r.t., 2–4 h.

Chart 2.   Synthesis of Pyridyl-Substituted 2-Vinyl Chromones

Table 2.   Inhibition Constants (K_i) of 2-Vinyl Chromone Derivatives for rMoPrP Aggregates

Compounds	K_i (nM)[a]	
	rMoPrP	Aβ_{1-42}
SC-NMe$_2$	7.61 (5.86)	21.8 (3.35)[b]
SC-NHEtOH	51.2 (18.1)	752 (78.9)
SC-NMeEtOH	88.0 (23.8)	106 (25.8)
VPC-NMe$_2$	>1000	>1000
VPC-OMe	>1000	>1000

a) K_i values of 2-vinyl chromone as determined by competitive binding assay using [^{125}I]SC-NMe$_2$ as a radioligand for rMoPrP aggregates or or Aβ_{1-42} aggregates. Each value is the mean (standard error of the mean) for three to six independent experiments. b) Data from ref. 26).

PrP^{Sc} models to screen efficient prion imaging probes.[19,21,22] The binding affinities of several SC derivatives for rMoPrP have been evaluated using [^{125}I]SC-NMe$_2$ which has the highest binding affinity among the series of SCs.[19] Therefore, we first investigated the binding affinity of chromone derivatives for rMoPrP aggregates by a competitive binding assay using [^{125}I]SC-NMe$_2$ as a radioligand (Table 2). The lead compound SC-NMe$_2$ showed strong binding affinity ($K_i = 7.61$ nM) for rMoPrP aggregates consistent with our previous reports.[19] SC-NHEtOH showed 6.7-fold lower binding affinity for rMoPrP ($K_i = 51.2$ nM) as compared with SC-NMe$_2$, indicating that the introduction of 2-hydroxyethyl group in the 4′-amino group diminish the binding affinity for rMoPrP aggregates but still maintained the binding interaction in some extent. As SC-NMeEtOH had a slightly lower affinity for rMoPrP aggregates ($K_i = 88.0$ nM) than SC-NHEtOH, introduction of a methyl group in the 4′-amino group seems to lead to reduce binding affinity to rMoPrP aggregates. Moreover, the binding affinity of chromone derivatives for Aβ_{1-42} aggregates was evaluated using a competitive binding assay with [^{125}I]SC-NMe$_2$. We found that SC-NHEtOH exhibited a weaker binding affinity for Aβ_{1-42} aggregates ($K_i = 752$ nM) than that of SC-NMe$_2$ ($K_i = 21.8$ nM[26]). The K_i value Aβ_{1-42} aggregates/rMoPrP aggregates ratio was 2.86 for SC-NMe$_2$ and 14.7 for SC-NHEtOH. Therefore, SC-NHEtOH has a lower affinity for Aβ_{1-42} and rMoPrP aggregates than SC-NMe$_2$ but is superior to Sc-NMe$_2$ in terms of selectivity for rMoPrP. The binding affinity of SC-NMeEtOH for Aβ_{1-42} was

higher ($K_i = 106$ nM) than that of SC-NHEtOH. The K_i value ratio of SC-NMeEtOH between rMoPrP aggregates and Aβ_{1-42} is 1.21, indicating no amyloid selectivity. Unfortunately, VPC-NMe$_2$ and VPC-OMe showed over 1000 nM of K_i values for both of rMoPrP aggregates and Aβ_{1-42} aggregates, indicating that displacement of styryl group at the 2-position of chromone by 2-(pyridin-3-yl)vinyl group completely abolished the binding affinity to amyloid aggregates. We and the others had reported that pyridyl benzofuran exhibited strong binding affinities to various amyloid species including PrP^{Sc}, amylin, and Aβ_{1-42} aggregates.[21,27,28] However, Song *et al.* reported that introduction of nitrogen atom in arylbenzofuran with 1-fluoro-3-(oxidanyl)propan-2-ol side chain decreased binding affinities to Aβ_{1-42} aggregates.[29] Although the reason for this discrepancy is unclear, it is suggested that the introduction of nitrogen to phenyl group prevents binding interaction between 2-vinyl chromones and PrP^{Sc} in this study. It is still unclear why none of the newly developed compounds showed a higher affinity for PrP^{Sc} as compared with lead compounds. However, according to our previous studies, SC derivatives tend to have a lower affinity for rMoPrP aggregates because of low lipophilicity.[19,21] Therefore, lipophilicity may have a strong effect on binding affinity for PrP^{Sc}.

As SC-NHEtOH has the highest binding affinity for rMoPrP among the newly developed 2-vinyl chromones in this study, we further examined whether SC-NHEtOH could recognize PrP^{Sc}-deposits in the brain tissue of prion infected mice. Thus, we evaluated the fluorescence imaging of SC-NHEtOH in the brain slices isolated from mBSE-infected and mock-infected mice according to our previous reports.[19,20] Fluorescence spots of SC-NHEtOH were detected in the brain section of mBSE-infected mice (Fig. 3A), confirming the co-staining of the region with PrP antibody (Fig. 3B). However, mock-infected mice did not show marked signal of SC-NHEtOH (Fig. 3C), consistently confirming the absence of PrP^{Sc} in the corresponding brain slice (Fig. 3D). These results indicated that SC-NHEtOH recognized the deposits consisting of PrP^{Sc} in the mouse brain.

In vitro studies demonstrated that SC-NHEtOH exhibited the moderate binding affinity for rMoPrP aggregates (Table 1) and it showed consistent distribution with PrP^{Sc}-positive regions in the mouse brain sections (Fig. 3). Accordingly, we further evaluated the usefulness of SC-NHEtOH as an
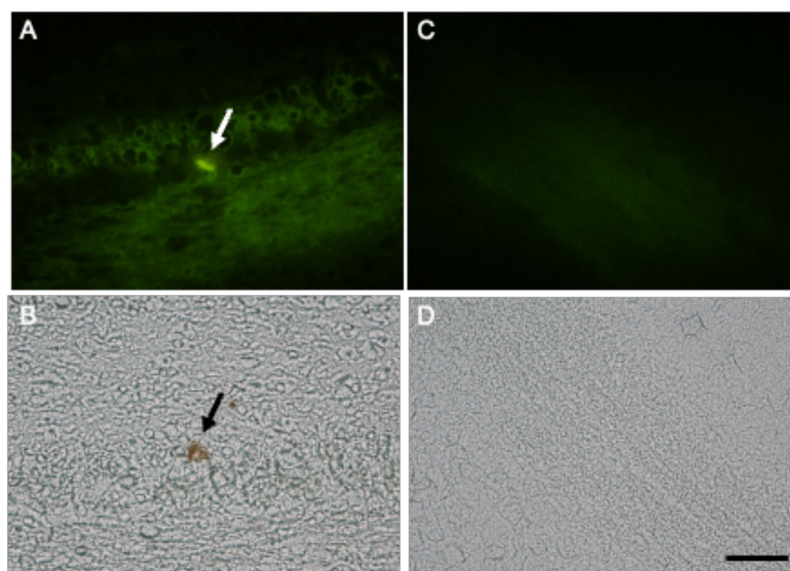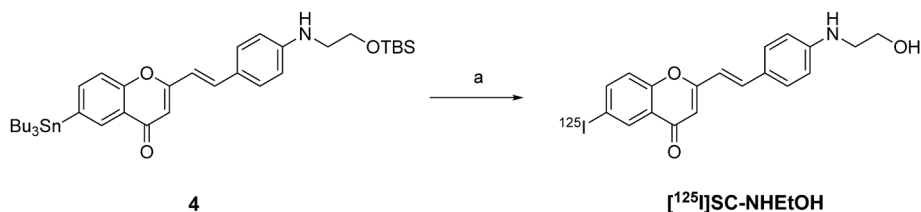
Fig. 3. Fluorescence Images of SC-NHEtOH in the Brain Slices from mBSE-Infected Mice (A) and Mock-Infected Mice (C)

Immunostaining images of PrP^Sc in adjacent slices with anti-PrP antibody (B and D, respectively). Scale bar represents 50 μm.

Reagents and conditions: (a) [^{125}I]NaI, H$_2$O$_2$, HCl, EtOH, r.t., 30 min.

Chart 3. Radioiodination of [^{125}I]SC-NHEtOH

Table 3. *In Vivo* Biodistribution after Intravenous Injection of [^{125}I]SC-NHEtOH into Normal Mice[a]

Organ	Time after injection (min)				
	2	30	60	120	180
Blood	8.79 (3.91)	1.86 (0.25)	1.31 (0.14)	1.11 (0.14)	1.03 (0.14)
Liver	30.81 (5.27)	17.24 (1.84)	11.42 (2.30)	9.70 (2.00)	9.29 (2.26)
Kidney	14.20 (2.06)	6.25 (0.89)	2.83 (0.56)	2.04 (0.20)	1.69 (0.22)
Intestine	1.03 (0.56)	6.98 (4.41)	5.60 (3.36)	6.00 (3.06)	7.53 (3.16)
Spleen	6.20 (0.68)	6.86 (1.45)	3.67 (1.10)	3.75 (1.05)	3.03 (1.16)
Lung	13.04 (3.64)	3.85 (0.61)	2.16 (0.42)	1.91 (0.54)	1.54 (0.33)
Stomach	1.67 (0.33)	2.06 (0.64)	2.04 (1.31)	2.12 (0.83)	2.18 (0.68)
Pancreas	4.47 (0.39)	1.57 (0.23)	1.32 (0.14)	1.21 (0.15)	1.15 (0.26)
Heart	6.37 (0.98)	1.60 (0.30)	1.02 (0.21)	0.82 (0.12)	0.77 (0.15)
Brain	0.88 (0.09)	0.44 (0.06)	0.35 (0.05)	0.29 (0.04)	0.26 (0.06)

a) Data are expressed as percent injected dose per gram (%ID/g). Each value is the mean (standard deviation) of five to seven mice.

imaging probe for PrP^Sc in the living brain. For i*n vivo* bio-distribution study, we next tried to prepare ^{125}I-labeled SC-NHEtOH. Although the radionuclide ^{123}I is used for SPECT diagnosis, we used ^{125}I (59.4 d) in this study instead of ^{123}I (13.3 h) for experimental convenience. Radioiodination of the [^{125}I]SC-NHEtOH was conducted by an iodo-destannylation reaction of TBS-protected tributyltin precursor 3 using hydrogen peroxide as an oxidant according to the method of our previous report regarding to the radiosynthesis of at yields of 15% (Chart 3).

Clinically available SPECT imaging agents for the prion

deposits should exhibit a high initial brain uptake and rapid clearance from non-target regions in the brain. Therefore, biodistribution studies of [^{125}I]SC-NHEtOH were conducted in normal mice and expressed as % of injected dose per gram (% ID/g) (Table 3). [^{125}I]SC-NHEtOH showed low initial brain uptake (0.88%ID/g at 2 min) of which gradually declined over time. The retained radioactivity of [^{125}I]SC-NHEtOH in the brain at 180 min was quite low (0.26% ID/g), indicating that this radioligand has no specific target molecules in the normal brain. It is well known that free radioiodine ions produced by deiodination are highly accumulated not only in the thy-

roid gland but also in the stomach.[30] Therefore, we selected stomach accumulation as an index of deiodination in this study. There was no marked increase in the [^{125}I]SC-NHEtOH uptake in stomach from 2 min (1.67% ID/g) to 180 min (2.18% ID/g), suggesting that no significant deiodination of [^{125}I]SC-NHEtOH occurred *in vivo*. We have reported that the lead compound [^{125}I]SC-NMe$_2$ showed slightly higher initial uptake (1.20% ID/g at 2 min) than that of [^{125}I]SC-NHEtOH. In addition, [^{125}I]SC-OMe showed about 2.5-fold higher brain uptake at 2 min than [^{125}I]SC-NHEtOH. The brain uptake at 2 min (brain$_{2\,min}$)/brain uptake at 60 min (brain$_{60\,min}$) ratio of normal mice is often used as an index parameter for comparing the washout rates of amyloid imaging probes. The brain$_{2\,min}$/brain$_{60\,min}$ ratio of [^{125}I]SC-NHEtOH is 2.5, which is higher as compared with [^{125}I]SC-NMe$_2$ (1.9), but much lower than [^{125}I]SC-OMe (4.0). The ratio of clinically useful PET probes such as [^{18}F]Florbetapir and [^{18}F]Florbetaben are 3.8[31] and 4.8,[32] respectively. The brain washout index parameter of [^{125}I]SC-NHEtOH seems to be inadequate for it to be used as an *in vivo* imaging agent for PrP^{Sc}. In addition, the initial brain uptake [^{18}F]Florbetapir and [^{18}F]Florbetaben at 2 min are much higher (4.90[31] and 7.77%[32] ID/g, respectively) as compared with [^{125}I]SC-NHEtOH. Accordingly, it is obvious that the BBB permeability of SC-NHEtOH is decisively lacking for clinical application. Relatively lower binding affinity of [^{125}I]SC-NHEtOH compared with our previously reported SPECT agents [^{123}I]SC-OMe and [^{123}I]IPBF-NHMe could humper the successful *in vivo* imaging of PrP^{Sc}. As demonstrated in Table 1, SC-NHEtOH has relatively low CNS PET MPO score (2.60) as compare with other 2-vinyl chromone derivatives that could contribute to inadequate brain uptake. Because SC-NMeEtOH has a higher CNS PET MPO score than SC-NHEtOH, it is expected to show better pharmacokinetics. However, the purpose of this study was to develop imaging agents for PrP^{Sc}. Therefore, we did not carry out *in vivo* animal experiments of [^{125}I]SC-NMeEtOH in this study to limit the number of animals used. Further structural modification based on [^{125}I]SC-NHEtOH to improve both of binding affinity for prion aggregates and brain pharmacokinetics may lead to more useful *in vivo* imaging probes of PrP^{Sc} deposits in the brain.

Conclusion

We have developed several 2-vinyl chromone derivatives with decreased lipophilicity and showed that SC-NHEtOH has a moderate binding affinity for PrP^{Sc}. [^{125}I]SC-NHEtOH showed poor initial brain uptake, although clearance from the brain was favorable. Further structural modification of SC-NHEtOH could make it useful imaging probe for visualization of prion deposits in the living brain.

Experimental

All reagents were commercially available and used without further purification. [^{125}I]NaI was purchased from PerkinElmer Life Sciences Inc. (Waltham, MA, U.S.A.). The ^{1}H NMR spectra were collected using a Varian Gemini 300 spectrometer or a JEOL JNM-AL 400 spectrometer. The mass spectra were collected on a JMS-T100TD or JMS-700N mass spectrometer (JEOL, Tokyo, Japan). HPLC analysis and purification were conducted using a Shimadzu HPLC system (LC-10AT pump with SPD-10A UV detector, $\lambda = 254$ nm). Gamma

counting was conducted using an automated gamma counter (2470 WIZARD^2, PerkinElmer.).

6-Bromo-2-(4-((2-*tert*-butyldimethylsilyl)oxy)ethyl)-amino)styryl)chromene-4-one (2) 6-Bromo-2-(4-aminostyryl)-chromone (**1**) was prepared according to the literature.[25] To a solution of **1** (300 mg, 0.876 mmol) N,N-dimethylformamide (DMF) (7.0 mL) were added K$_2$CO$_3$ (610 mg, 4.41 mmol) and (2-bromoethoxy)-*tert*-butyldimethyl-silane (735 μL, 3.51 mmol) and then the mixture was heated at 70 °C for 8 h. The reaction mixture was cooled, added to satd. NaHCO$_3$ and extracted twice with EtOAc. The organic layers were combined, washed with brine, evaporated, and dried *in vacuo*. The crude product was subjected to chromatographic purification on silica gel using CHCl$_3$/EtOAc (9 : 1) to give **2** (181 mg, 41%) as a yellow powder. ^{1}H-NMR (400 MHz, CDCl$_3$) δ: 0.08 (s, 6H), 0.92 (s, 9H), 3.28 (t, $J = 5.4$ Hz, 2H), 3.84 (t, $J = 6.8$ Hz, 2H) 4.44 (s, 1H), 6.25 (s, 1H), 6.55 (d, $J = 16.0$ Hz, 1H), 6.63 (d, $J = 8.4$ Hz, 2H), 7.39–7.56 (m, 4H), 7.73 (dd, $J = 2.4$, 8.8 Hz, 1H), 8.31 (d, $J = 2.4$ Hz, 1H). MS (Direct Analysis in Real Time (DART)) *m/z*: 500, 502 (M$^+$).

(E)-6-Bromo-2-(4-((2-((*tert*-butyldimethylsilyl)oxy)ethyl)-(methyl)amino) Styryl)-4*H*-chromen-4-one (3) To a solution of **2** (412 mg, 0.82 mmol) in CH$_3$CO$_2$H (10 mL) were added paraformaldehyde (505 mg, 16.8 mmol) and sodium sodium cyanoborohydride (813 mg, 12.9 mmol) and then the mixture was stirred at room temperature for 3 h. The reaction mixture was quenched by satd. NaHCO$_3$, extracted with CHCl$_3$ and washed with brine. The organic layer was dried over Na$_2$SO$_4$, evaporated and dried *in vacuo*. The crude product was subjected to chromatographic purification on silica gel using EtOAc/hexane (1 : 2) to give **3** (214 mg, 51%) as a yellow powder. ^{1}H-NMR (400 MHz, CDCl$_3$) δ: 0.02 (s, 6H), 0.86 (s, 9H), 3.07 (s, 3H), 3.54 (t, $J = 5.6$ Hz, 2H), 3.80 (t, $J = 6.4$ Hz, 2H), 6.24 (s, 1H), 6.53 (d, $J = 16.4$ Hz, 1H), 6.70 (d, $J = 8.8$ Hz, 2H), 7.40 (d, $J = 8.8$ Hz, 1H), 7.50 (d, $J = 8.8$ Hz, 2H), 7.52 (d, $J = 16.4$ Hz, 1H), 7.74 (dd, $J = 8.8$, 2.8 Hz, 1H), 8.31 (d, $J = 2.4$ Hz, 1H). MS (DART) *m/z*: 514 (M$^+$).

6-(Tributylstannyl)-2-(4-((2-((*tert*-butyldimethylsilyl)oxy)-ethyl)amino)styryl) Chromene-4-one (4) To a solution of **2** (20 mg, 40.1 μmol) in a solvent mixture (3.3 mL, 3 : 2 dioxane/Et$_3$N) were added bis(tributyltin) (21.1 μL, 41.8 μmol) and Pd(PPh$_3$)$_4$ (4.81 mg, 4.16 μmol) and then the mixture was heated at 90 °C for 7 h. After cooling to the room temperature, the reaction mixture was evaporated to dryness. The residue was subjected to chromatographic purification on silica gel using EtOAc/hexane (3 : 1) to give **4** (5.0 mg, 18%) as a red powder. ^{1}H-NMR (400 MHz, CDCl$_3$) δ: 0.08 (s, 6H), 0.081–0.888 (m, 9H), 0.92 (s, 9H), 1.10–1.11 (m, 6H), 1.30–1.36 (m, 6H), 1.48–1.53 (m, 6H), 3.28 (t, $J = 5.2$ Hz, 2H), 3.84 (t, $J = 5.2$ Hz, 2H), 6.27 (s, 1H), 6.56 (d, $J = 16.0$ Hz, 1H), 6.63 (d, $J = 8.8$ Hz, 2H), 7.33 (d, $J = 8.8$ Hz, 1H), 7.44 (d, $J = 8.4$ Hz, 2H), 7.52 (d, $J = 16.8$ Hz, 1H), 7.72 (dd, $J = 6.8$, 3.2 Hz, 1H), 8.26 (dd, $J = 4.8$, 1.2 Hz, 1H). MS (DART) *m/z*: 710 (M + H).

(E)-2-(4-((2-((*tert*-Butyldimethylsilyl)oxy)ethyl)(methyl)-amino)styryl)-6-(tributylstannyl)-4*H*-chromen-4-one (5) To a solution of **3** (214 mg, 0.46 mmol) in a solvent mixture (7.0 mL, 3 : 1 dioxane/Et$_3$N) were added bis(tributyltin) (1.69 mL, 3.56 mmol) and Pd(PPh$_3$)$_4$ (85.6 mg, 74.1 μmol) and then the mixture was heated at 90 °C for 12 h. After cooling to the room temperature, the reaction mixture was evaporated to dryness. The residue was subjected to chromatographic

purification on silica gel using EtOAc/hexane (3 : 1) to give **5** (69 mg, 23%) as a yellow powder. ^{1}H-NMR (400 MHz, CDCl$_3$) δ: 0.02 (s, 6H), 0.88 (s, 9H), 1.09–1.13 (m, 6H), 1.31–1.39 (m, 6H), 1.50–1.58 (m, 6H), 3.06 (s, 3H), 3.53 (t, $J = 5.6$ Hz, 2H), 3.80 (t, $J = 6.4$ Hz, 2H), 6.27 (s, 1H), 6.55 (d, $J = 16.0$ Hz, 1H), 6.70 (d, $J = 9.2$ Hz, 2H), 7.46 (d, $J = 8.4$ Hz, 2H), 7.53 (d, $J = 15.6$ Hz, 1H), 7.73 (d, $J = 6.8$ Hz, 1H), 8.28 (s, 1H). MS (DART) *m/z*: 724 (M + H$^+$).

6-Iodo-2-(4-((2-((*tert*-butyldimethylsilyl)oxy)ethyl)amino)-styryl)chromene-4-one (6) To a solution of **4** (132 mg, 0.19 mmol) in CHCl$_3$ (3.0 mL) was added a solution of iodine in CHCl$_3$ (2.0 mL, 0.2 M) and then the mixture was stirred at room temperature for 2 h. The reaction mixture was quenched by satd. NaHSO$_3$ (10 mL) and extracted twice with CHCl$_3$. The organic layers were combined, washed with brine, evaporated, and dried *in vacuo*. The crude product was subjected to chromatographic purification on silica gel using CHCl$_3$/EtOAc/Et$_3$N (25 : 75 : 1) to give **6** (46 mg, 45%) as a reddish-brown powder. ^{1}H-NMR (400 MHz, CDCl$_3$) δ: 0.08 (s, 6H), 0.91 (s, 9H), 3.28 (t, $J = 5.4$ Hz, 2H), 3.82 (s, 1H), 3.84 (t, $J = 5.2$ Hz, 2H), 6.25 (s, 1H), 6.54 (d, $J = 15.6$ Hz, 1H), 6.63 (d, $J = 8.8$ Hz, 2H), 7.30 (d, $J = 15.6$ Hz, 1H), 7.43 (d, $J = 8.4$ Hz, 2H), 7.52 (d, $J = 16.0$ Hz, 1H), 7.91 (dd, $J = 8.8, 2.4$ Hz, 1H), 8.51 (d, $J = 2.0$ Hz, 1H). MS (DART) *m/z*: 548(M + H$^+$).

(*E*)-2-(4-((*tert*-Butyldimethylsilyl)oxy)ethyl)(methyl)-amino)styryl)-6-iodo-4*H*-chromen-4-one (7) To a solution of **5** (55 mg, 75.7 µmol) in CHCl$_3$ (1.5 mL) was added a solution of iodine in CHCl$_3$ (1.0 mL, 0.2 M) and then the mixture was stirred at room temperature for 1 h. The reaction mixture was quenched by satd. NaHSO$_3$ (10 mL) and extracted twice with CHCl$_3$. The organic layers were combined, washed with brine, evaporated, and dried *in vacuo*. The crude product was subjected to chromatographic purification on silica gel using CHCl$_3$/EtOAc (4 : 1) to give **7** (31 mg, 73%) as a reddish-brown powder. ^{1}H-NMR (400 MHz, CDCl$_3$) δ: 0.02 (s, 6H), 0.88 (s, 9H), 3.07 (s, 3H), 3.54 (t, $J = 5.2$ Hz, 2H), 3.80 (t, $J = 5.2$ Hz, 2H), 6.23 (s, 1H), 6.52 (d, $J = 15.6$ Hz, 1H), 6.69 (d, $J = 8.4$ Hz, 2H), 7.44 (d, $J = 8.8$ Hz, 2H), 7.51 (d, $J = 16.0$ Hz, 1H), 7.89 (d, $J = 6.8$ Hz, 1H), 8.50 (s, 1H). MS (DART) *m/z*: 561 (M + H$^+$).

(*E*)-2-(4-((2-Hydroxyethyl)amino)styryl)-6-iodo-4*H*-chromen-4-one (SC-NHEtOH) To a solution of **6** (46 mg, 84.1 µmol) in tetrahydrofuran (THF) (8.0 mL) was added tetrabutylammonium fluoride in THF (2.66 mL, 1.0 M), and the reaction was allowed to proceed at room temperature for 1 h. The reaction mixture was quenched by satd. NH$_4$Cl aq (10 mL), followed by extraction twice with CHCl$_3$. The organic layers were combined, dried with Na$_2$SO$_4$, evaporated, and dried *in vacuo*. The crude product was subjected to chromatographic purification on silica gel using CHCl$_3$/MeOH (49 : 1) to give SC-NHEtOH (8.0 mg, 22%) as a reddish-brown powder. ^{1}H-NMR (400 MHz, CDCl$_3$) δ: 3.38 (t, $J = 5.2$ Hz, 2H), 3.89 (t, $J = 4.8$ Hz, 2H), 4.30 (s, 1H), 6.24 (s, 1H), 6.53 (d, $J = 16.0$ Hz, 1H), 6.65 (d, $J = 8.8$ Hz, 2H), 7.25 (s, 1H), 7.30 (d, $J = 4.4$ Hz, 1H), 7.43 (d, $J = 8.4$ Hz, 2H), 7.51 (d, $J = 16.0$ Hz, 1H), 7.91 (dd, $J = 8.4, 2.0$ Hz, 1H), 8.51 (d, $J = 2.4$ Hz, 1H). High resolution (HR) MS (FAB) *m/z*: calcd for C$_{19}$H$_{17}$INO$_3$ (M + H$^+$)434.0253, found 434.0248.

(*E*)-2-(4-((2-Hydroxyethyl)(methyl)amino)styryl)-6-iodo-4*H*-chromen-4-one (SC-NMeEtOH) To a solution of **7** (45 mg, 80.2 µmol) in THF (4.0 mL) was added tetrabutylammonium fluoride in THF (1.5 mL, 1.0 M), and it reacted at

room temperature for 2 h. The reaction mixture was quenched by satd. NH$_4$Cl aq (5.0 mL), followed by extraction twice with CHCl$_3$. The organic layers were combined, dried with Na$_2$SO$_4$, evaporated and dried *in vacuo*. The crude product was subjected to chromatographic purification on silica gel using CHCl$_3$/MeOH (49 : 1) to give SC-NMeEtOH (22 mg, 58%) as a reddish-brown powder. ^{1}H-NMR (400 MHz, CDCl$_3$) δ: 3.07 (s, 3H), 3.54 (t, $J = 6.4$ Hz, 2H), 3.80 (t, $J = 5.6$ Hz, 2H), 6.23 (s, 1H), 6.52 (d, $J = 15.6$ Hz, 1H), 6.69 (d, $J = 8.4$ Hz, 2H), 7.44 (d, $J = 8.8$ Hz, 2H), 7.51 (d, $J = 16.0$ Hz, 1H), 7.89 (d, $J = 6.8$ Hz, 1H), 8.50 (s, 1H). HRMS (FAB) *m/z*: calcd for C$_{20}$H$_{19}$INO$_3$ (M + H$^+$) 448.0410, found 448.0410.

(*E*)-6-Bromo-2-(2-(6-(dimethylamino)pyridin-3-yl)vinyl)-4*H*-chromen-4-one (8) To a solution of 6-bromo-2-methyl-chromone (159 mg, 0.67 mmol) in EtOH (10 mL) were added 6-(*N*,*N*-dimethylamino)nicotinaldehyde (150 mg, 1.00 mmol) and KOH (91.4 mg, 3.33 mmol) and then the mixture was stirred was heated at 50 °C for 3 h. After cooling to the room temperature, the reaction mixture was quenched by 1 M HCl, followed by extraction with CHCl$_3$ twice. The organic layers were combined, dried with Na$_2$SO$_4$, evaporated, and dried *in vacuo*. The residue was subjected to chromatographic purification on silica gel using CHCl$_3$/MeOH (49 : 1) to give **8** (220 mg, 89%) as an ocher powder. ^{1}H-NMR (400 MHz, CDCl$_3$) δ: 3.18 (s, 6H), 6.26 (s, 1H), 6.53 (d, $J = 16.4$ Hz, 1H), 6.57 (d, $J = 9.2$ Hz, 1H), 7.43 (d, $J = 9.2$ Hz, 1H), 7.51 (d, $J = 16.0$ Hz, 1H), 7.70–7.76 (m, 2H), 8.31 (d, $J = 2.4$ Hz, 2H). MS (DART) *m/z*: 371, 373 (M + H$^+$).

(*E*)-6-Bromo-2-(2-(6-methoxypyridin-3-yl)vinyl)-4*H*-chromen-4-one (9) To a solution of 6-bromo-2-methyl-chromone (230 mg, 0.96 mmol) in EtOH (10 mL) were added 6-methoxynicotinaldehyde (400 mg, 2.9 mmol) and KOH (539 mg, 9.60 mmol) and then the mixture was heated at 70 °C for 4 h. After cooling to the room temperature, the reaction mixture was quenched by 1 M HCl, followed by extraction twice with EtOAc. The organic layers were combined, dried with Na$_2$SO$_4$, evaporated, and dried *in vacuo*. The residue was subjected to chromatographic purification on silica gel using CHCl$_3$ to give **9** (277 mg, 80%) as an ocher powder. ^{1}H-NMR (400 MHz, CDCl$_3$) δ: 3.99 (s, 3H), 6.31 (s, 1H), 6.69 (d, $J = 16.4$ Hz, 1H), 6.82 (d, $J = 8.8$ Hz, 1H), 7.47 (d, $J = 6.4$ Hz, 1H), 7.56 (d, $J = 16.0$ Hz, 1H), 7.77 (dd, $J = 11.4, 2.8$ Hz, 1H), 7.86 (dd, $J = 8.8, 2.4$ Hz, 1H), 8.32 (d, $J = 2.8$ Hz, 2H). MS (DART) *m/z*: 357, 379 (M + H$^+$).

(*E*)-2-(2-(6-(Dimethylamino)pyridin-3-yl)vinyl)-6-(tributylstannyl)-4*H*-chromen-4-one (10) To a solution of **8** (220 mg, 0.59 mmol) in a solvent mixture (17 mL, 3 : 1 dioxane/Et$_3$N) were added bis(tributyltin) (1.12 mL, 2.89 mmol) and Pd(PPh$_3$)$_4$ (67.9 mg, 58.7 µmol) and then the mixture was heated at 90 °C for 11 h. After cooling to the room temperature, the reaction mixture was evaporated to dryness. The residue was subjected to chromatographic purification on silica gel using EtOAc/hexane (1 : 2) to give **10** (90 mg, 29%) as a yellow oil. ^{1}H-NMR (400 MHz, CDCl$_3$) δ: 0.89 (t, $J = 12.8$ Hz, 9H), 1.09–1.13 (m, 6H), 1.31–1.39 (m, 6H), 1.50–1.58 (m, 6H), 3.17 (s, 6H), 6.27 (s, 1H), 6.55 (d, $J = 16.4$ Hz, 1H), 6.57 (d, $J = 9.2$ Hz, 1H), 7.51 (d, $J = 16.0$ Hz, 1H), 7.73–7.75 (m, 2H), 7.92 (dd, $J = 8.8, 2.4$ Hz, 1H), 8.27 (d, $J = 0.8$ Hz, 1H), 8.31 (d, $J = 2.0$ Hz, 1H), 8.56 (d, $J = 2.0$ Hz, 1H). MS (DART) *m/z*: 583 (M + H$^+$).

(*E*)-2-(2-(6-Methoxypyridin-3-yl)vinyl)-6-(tributylstannyl)-

4*H*-chromen-4-one (11) To a solution of **9** (185 mg, 0.78 mmol) in a solvent mixture (3.3 mL, 3 : 2 dioxane/Et$_3$N) were added bis(tributyltin) (0.93 mL, 2.40 mmol) and Pd(PPh$_3$)$_4$ (87.9 mg, 76.1 μmol) and then the mixture was heated at 90 °C for 8 h. After cooling to the room temperature, the reaction mixture was evaporated to dryness. The residue was subjected to chromatographic purification on silica gel using CHCl$_3$/EtOAc (9 : 1) to give **11** (25 mg, 6%) as a yellow oil. ^{1}H-NMR (400 MHz, CDCl$_3$) δ: 0.89 (t, *J* = 14.8 Hz, 9H), 1.03–1.16 (m, 6H), 1.29–1.40 (m, 6H), 1.56–1.42 (m, 6H), 3.99 (s, 3H), 6.32 (s, 1H), 6.68 (d, *J* = 16.0 Hz, 1H), 6.82 (d, *J* = 8.8 Hz, 1H), 7.49 (d, *J* = 8.0 Hz, 1H), 7.55 (d, *J* = 16.0 Hz, 1H), 7.76 (dd, *J* = 8.2, 1.2 Hz, 1H), 7.85 (dd, *J* = 8.8, 2.4 Hz, 1H), 8.28 (d, *J* = 0.80 Hz, 1H), 8.33 (d, *J* = 2.0 Hz, 1H). MS (DART) *m/z*: 568 (M + H$^+$).

(*E*)-2-(2-(6-(Dimethylamino)pyridin-3-yl)vinyl)-6-iodo-4*H*-chromen-4-one (VPC-NMe$_2$) To a solution of **10** (43 mg, 77.7 μmol) in CHCl$_3$ (1.5 mL) was added a solution of iodine in CHCl$_3$ (1.0 mL, 0.2 M) and then the mixture was stirred at room temperature for 2 h. The reaction mixture was quenched by satd. NaHSO$_3$ (10 mL) and extracted twice with CHCl$_3$. The organic layers were combined, washed with brine, evaporated, and dried *in vacuo*. The crude product was subjected to chromatographic purification on silica gel using EtOAc/hexane (1 : 2) to give VPC-NMe$_2$ (30 mg, 97%) as a yellow powder. ^{1}H-NMR (400 MHz, CDCl$_3$) δ: 3.17 (s, 6H), 6.26 (s, 1H), 6.53 (d, *J* = 16.0 Hz, 1H), 6.57 (d, *J* = 9.2 Hz, 1H), 7.30 (d, *J* = 8.8 Hz, 1H), 7.50 (d, *J* = 16.0 Hz, 1H), 7.73 (dd, *J* = 9.2, 2.4 Hz, 1H), 7.92 (dd, *J* = 8.8, 1.6 Hz, 1H), 8.31 (d, *J* = 2.4 Hz, 1H), 8.51 (d, *J* = 2.4 Hz, 1H). HRMS (FAB) *m/z*: calcd for C$_{18}$H$_{16}$IN$_2$O$_2$ (M + H$^+$) 419.0256, found 419.0257.

(*E*)-6-Iodo-2-(2-(6-methoxypyridin-3-yl)vinyl)-4*H*-chromen-4-one (VPC-OMe) To a solution of **11** (17 mg, 31.5 μmol) in EtOAc (1.0 mL) was added a solution of iodine in EtOAc (0.5 mL, 0.2 M) and then the mixture was stirred at room temperature for 4 h. The reaction mixture was quenched by satd. NaHSO$_3$ (5.0 mL) and extracted twice with EtOAc. The organic layers were combined, washed with brine, evaporated, and dried *in vacuo*. The crude product was subjected to chromatographic purification on silica gel using EtOAc/hexane (1 : 3) to give VPC-OMe (11 mg, 91%) as a brown powder. ^{1}H-NMR (400 MHz, CDCl$_3$) 3.99 (s, 3H), 6.31 (s, 1H), 6.67 (d, *J* = 16.0 Hz, 1H), 6.82 (d, *J* = 8.8 Hz, 1H), 7.32 (d, *J* = 8.8 Hz, 1H), 7.55 (d, *J* = 16.0 Hz, 1H), 7.86 (dd, *J* = 8.8, 2.8 Hz, 1H), 7.95 (dd, *J* = 8.8, 1.2 Hz, 1H), 8.32 (d, *J* = 2.4 Hz, 1H), 8.52 (d, *J* = 2.4 Hz, 1H). HRMS (FAB) *m/z*: calcd for C$_{17}$H$_{13}$INO$_3$ (M + H$^+$) 405.9940, found 405.9940.

Radiochemistry The [^{125}I]SC-NHEtOH was synthesized according to our previous report.[33] In brief, a solution of tributyltin derivative **4** (50 μg) in 50 μL of EtOH was added [^{125}I]NaI (3.7 − 7.4 MBq, molar activity = 78.6 GBq/μmol), 1 M HCl (50 μL), and 50 μL of H$_2$O$_2$ (3%). The reaction mixture was incubated at room temperature for 30 min, after which NaHSO$_3$ was added. The mixture was quenched with 1.0 M NaOH (400 μL) and extracted with EtOAc. The organic layer was dried with an anhydrous Na$_2$SO$_4$ column, and then dried with N$_2$ gas. The radioiodinated ligand [^{125}I]SC-NHEtOH was purified by HPLC on a Cosmocil 5C$_{18}$-AR-II column (4.6 × 150 mm; Nacalai Tesque Inc., Kyoto, Japan.) at a flow rate of 1.0 mL/min with an isocratic mobile phase of 50% acetonitrile in water.

Competitive Binding Assay Using rMoPrP Aggregates Expression and aggregation of rMoPrP were performed as described previously.[10,34,35] Binding assays for 2-vinyl chromone derivatives and rMoPrP aggregates were performed according to our previous study.[19,21] Briefly, the mixture contained [^{125}I]SC-NMe$_2$ (0.02 nM), test compound (4.0 pM–1.0 μM), and rMoPrP aggregates (100 nM) in NaCl/*N*-(2-hydroxyethyl)-piperazine-*N*′-2-ethanesulfonic acid (HEPES) buffer (50 mM HEPES/KOH, 300 mM NaCl, pH 7.5) containing 20% (v/v) dimethyl sulfoxide (DMSO). After incubation for 2 h at room temperature, the mixture was filtered through Whatman GF/B filters using a Brandel M-24 cell harvester and the filtrates quantified using a gamma counter. Nonspecific binding was measured in the presence of 500 nM non-radioactive SC-NMe$_2$. Values for the IC$_{50}$ were determined from displacement curves of three independent experiments using PRISM4 (GraphPad Software Inc., San Diego, CA, USA.), and those for the K_i were calculated using the Cheng–Prusoff equation.

Ethics Statement Experiments using animals were conducted in accordance with our institutional guidelines and were ap-proved by the Nagasaki University Animal Care Committee (Approval number; 1211201033-5).

Animals All animals were obtained from commercial supplier Kyudo Co., Ltd. (Saga, Japan). The mBSE infectious animal experiment was performed at biosafety level 3 (BSL3) containment in accordance with the institutional guidelines as previously reported.[36,37]

Fluorescence Staining of mBSE-Infected and Mock-infected Mouse Brain Sections Fluorescence staining experiments were performed as described previously.[19,21,22] In brief, 10 μm of serial sections from frozen brain tissues were incubated with a 50% EtOH solution containing SC-NHEtOH (100 μM) for 24 h. Each section was washed twice with 50% EtOH. Fluorescence images were captured using an Eclipse 80i microscope (Nikon Corp., Tokyo, Japan) with a B-2A filter set (excitation: 450–490 nm; dichromic mirror: 505 nm; long-pass filter: 520 nm). Immunohistochemical staining of adjacent slices was performed using SAF32 anti-PrP antibody (Bertin Bioreagent, Montigny-le-Bretonneux, France, No. A03202) (1 : 20) as the primary antibody and anti-mouse biotinylated antibody as the secondary antibody. The signal was visualized by a reaction with hydrogen peroxidase-activated diaminobenzidine.

***In Vivo* Biodistribution in Normal Mice** A saline solution containing 20% DMSO of [^{125}I]SC-NHEtOH (7.4 kBq, 100 μL) was intravenously injected into ddY mice (male, 5 weeks old, 20−25 g). The mice were sacrificed at each time point post-injection. After dissecting and weighing the organs, a gamma counter (PerkinElmer, 2470 WIZARD^2) was used to measure the radioactivity of the organs.

Conflict of Interest The authors declare no conflict of interest.

References

1) Eraña H., Charco J. M., González-Miranda E., García-Martínez S., López-Moreno R., Pérez-Castro M. A., Díaz-Domínguez C. M., García-Salvador A., Castilla J., *Biomolecules*, **10**, 469 (2020).

2) Colby D. W., Prusiner S. B., *Cold Spring Harb. Perspect. Biol.*, **3**, 1–22 (2011).

3) Budka H., *Br. Med. Bull.*, **66**, 121–130 (2003).

4) Soto C., *Cell*, **149**, 968–977 (2012).

5) Kraus A., Groveman B. R., Caughey B., *Annu. Rev. Microbiol.*, **67**, 543–564 (2013).

6) Ureshino R. P., Erustes A. G., Bassani T. B., Wachilewski P., Guarache G. C., Nascimento A. C., Costa A. J., Smaili S. S., da Silva Pereira G. J., *Int. J. Mol. Sci.*, **20**, 6004 (2019).

7) Puoti G., Bizzi A., Forloni G., Safar J. G., Tagliavini F., Gambetti P., *Lancet Neurol.*, **11**, 618–628 (2012).

8) Bongianni M., Orrù C., Groveman B. R., *et al.*, *JAMA Neurol.*, **74**, 155–162 (2017).

9) Orrú C. D., Bongianni M., Tonoli G., Ferrari S., Hughson A. G., Groveman B. R., Fiorini M., Pocchiari M., Monaco S., Caughey B., Zanusso G., *N. Engl. J. Med.*, **371**, 519–529 (2014).

10) Atarashi R., Satoh K., Sano K., Fuse T., Yamaguchi N., Ishibashi D., Matsubara T., Nakagaki T., Yamanaka H., Shirabe S., Yamada M., Mizusawa H., Kitamoto T., Klug G., McGlade A., Collins S. J., Nishida N., *Nat. Med.*, **17**, 175–178 (2011).

11) Wadsworth J. D., Collinge J., *Acta Neuropathol.*, **121**, 69–77 (2011).

12) Watanabe R., Duchen L. W., *Neuropathol. Appl. Neurobiol.*, **19**, 253–260 (1993).

13) Fuchigami T., *Yakugaku Zasshi*, **139**, 1531–1538 (2019).

14) Ono M., *Chem. Pharm. Bull.*, **57**, 1029–1039 (2009).

15) Rambaran R. N., Serpell L. C., *Prion*, **2**, 112–117 (2008).

16) Letourneau-Guillon L., Wada R., Kucharczyk W., *J. Magn. Reson. Imaging*, **35**, 998–1012 (2012).

17) Deters K. D., Risacher S. L., Yoder K. K., Oblak A. L., Unverzagt F. W., Murrell J. R., Epperson F., Tallman E. F., Quaid K. A., Farlow M. R., Saykin A. J., Ghetti B., *Am. J. Nucl. Med. Mol. Imaging*, **6**, 84–93 (2016).

18) Okamura N., Shiga Y., Furumoto S., Tashiro M., Tsuboi Y., Furukawa K., Yanai K., Iwata R., Arai H., Kudo Y., Itoyama Y., Doh-ura K., *Eur. J. Nucl. Med. Mol. Imaging*, **37**, 934–941 (2010).

19) Fuchigami T., Yamashita Y., Kawasaki M., Ogawa A., Haratake M., Atarashi R., Sano K., Nakagaki T., Ubagai K., Ono M., Yoshida S., Nishida N., Nakayama M., *Sci. Rep.*, **5**, 18440 (2016).

20) Kawasaki M., Fuchigami T., Kobashi N., Nakagaki T., Sano K., Atarashi R., Yoshida S., Haratake M., Nishida N., Nakayama M., *Bioorg. Med. Chem.*, **25**, 1085–1093 (2017).

21) Fuchigami T., Kawasaki M., Watanabe H., Nakagaki T., Nishi K., Sano K., Atarashi R., Nakaie M., Yoshida S., Ono M., Nishida N., Nakayama M., *Nucl. Med. Biol.*, **90–91**, 41–48 (2020).

22) Fuchigami T., Kawasaki M., Koyama R., Nakaie M., Nakagaki T., Sano K., Atarashi R., Yoshida S., Haratake M., Ono M., Nishida N., Nakayama M., *ACS Infect. Dis.*, **5**, 2003–2013 (2019).

23) Zhang L., Villalobos A., Beck E. M., Bocan T., Chappie T. A., Chen L., Grimwood S., Heck S. D., Helal C. J., Hou X., Humphrey J. M., Lu J., Skaddan M. B., McCarthy T. J., Verhoest P. R., Wager T. T., Zasadny K., *J. Med. Chem.*, **56**, 4568–4579 (2013).

24) Wager T. T., Hou X., Verhoest P. R., Villalobos A., *ACS Chem. Neurosci.*, **1**, 435–449 (2010).

25) Ono M., Maya Y., Haratake M., Nakayama M., *Bioorg. Med. Chem.*, **15**, 444–450 (2007).

26) Fuchigami T., Ogawa A., Yamashita Y., Haratake M., Watanabe H., Ono M., Kawasaki M., Yoshida S., Nakayama M., *Bioorg. Med. Chem. Lett.*, **25**, 3363–3367 (2015).

27) Watanabe H., Kawano K., Iikuni S., Shimizu Y., Ono M., *Nucl. Med. Biol.*, **90–91**, 93–97 (2020).

28) Ono M., Cheng Y., Kimura H., Watanabe H., Matsumura K., Yoshimura M., Iikuni S., Okamoto Y., Ihara M., Takahashi R., Saji H., *PLOS ONE*, **8**, e74104 (2013).

29) Song J., Zhang X., Zhao Y., Yang H., Zhang J., Zhang X., Dai J., Cui M., *Eur. J. Med. Chem.*, **134**, 271–280 (2017).

30) Garg P. K., Harrison C. L., Zalutsky M. R., *Cancer Res.*, **50**, 3514–3520 (1990).

31) Yoshimura M., Ono M., Matsumura K., Watanabe H., Kimura H., Cui M., Nakamoto Y., Togashi K., Okamoto Y., Ihara M., Takahashi R., Saji H., *ACS Med. Chem. Lett.*, **4**, 596–600 (2013).

32) Zhang W., Oya S., Kung M. P., Hou C., Maier D. L., Kung H. F., *Nucl. Med. Biol.*, **32**, 799–809 (2005).

33) Fuchigami T., Kobashi N., Haratake M., Kawasaki M., Nakayama M., *Eur. J. Med. Chem.*, **60**, 469–478 (2013).

34) Atarashi R., Moore R. A., Sim V. L., Hughson A. G., Dorward D. W., Onwubiko H. A., Priola S. A., Caughey B., *Nat. Methods*, **4**, 645–650 (2007).

35) Sano K., Atarashi R., Ishibashi D., Nakagaki T., Satoh K., Nishida N., *J. Virol.*, **88**, 11791–11801 (2014).

36) Fujihara A., Atarashi R., Fuse T., Ubagai K., Nakagaki T., Yamaguchi N., Ishibashi D., Katamine S., Nishida N., *FEBS J.*, **276**, 2841–2848 (2009).

37) Nakagaki T., Satoh K., Ishibashi D., Fuse T., Sano K., Kamatari Y. O., Kuwata K., Shigematsu K., Iwamaru Y., Takenouchi T., Kitani H., Nishida N., Atarashi R., *Autophagy*, **9**, 1386–1394 (2013).